Nanotechnology **19** (2008) 255606 (7pp) doi:10.1088/0957-4484/19/25/255606

Synthesis of novel magnetic iron metal–silica (Fe–SBA-15) and magnetite–silica (Fe_3O_4–SBA-15) nanocomposites with a high iron content using temperature-programed reduction

H H P Yiu[1,2], M A Keane[3], Z A D Lethbridge[4], M R Lees[5], A J El Haj[2] and J Dobson[2]

[1] Department of Chemistry, University of Liverpool, Liverpool, Merseyside L69 7ZD, UK
[2] Institute of Science and Technology in Medicine, Keele University, Thornburrow Drive, Hartshill, Stoke-on-Trent ST4 7QB, UK
[3] Chemical Engineering, School of Engineering and Physical Sciences, Heriot-Watt University, Edinburgh EH14 4AS, UK
[4] Department of Chemistry, University of Warwick, Gibbet Hill Road, Coventry CV4 7AL, UK
[5] Department of Physics, The University of Warwick, Gibbet Hill Road, Coventry CV4 7AL, UK

E-mail: j.p.dobson@keele.ac.uk

Received 25 March 2008, in final form 15 April 2008
Published 15 May 2008
Online at stacks.iop.org/Nano/19/255606

Abstract

Magnetic iron metal–silica and magnetite–silica nanocomposites have been prepared via temperature-programed reduction (TPR) of an iron oxide–SBA-15 (SBA: Santa Barbara Amorphous) composite. TPR of the starting SBA-15 supported Fe_2O_3 generated Fe_3O_4 and FeO as stepwise intermediates in the ultimate formation of Fe–SBA-15. The composite materials have been characterized by means of x-ray diffraction, high resolution transmission electron microscopy and SQUID (superconducting quantum interference device) magnetometry. The Fe oxide and metal components form a core, as nanoscale particles, that is entrapped in the SBA-15 pore network. Fe_3O_4–SBA-15 and Fe–SBA-15 exhibited superparamagnetic properties with a total magnetization value of 17 emu g^{-1}. The magnetite–silica composite (at an Fe_3O_4 loading of 30% w/w) delivered a magnetization that exceeded values reported in the literature or obtained with commercial samples. Due to the high pore volume of the mesoporous template, the magnetite content can be increased to 83% w/w with a further enhancement of magnetization.

1. Introduction

The importance of functionalized magnetic nanoparticles in medical applications has already been established in, for example, magnetic resonance imaging (MRI) [1], drug delivery [2], cell sorting [3] and gene therapy [4]. Conventional preparation of these nanoparticles typically involves coating iron oxide crystallites (usually magnetite (Fe_3O_4) or maghemite (γ-Fe_2O_3)), prepared by precipitation or vapor deposition, with a polymer. Functional groups can then be tethered to the surface for the purpose of attaching/carrying drug and DNA molecules [5]. Silica is also a suitable coating material due to the high associated mechanical strength and facile functionalization via silylation. However, coating silica onto iron oxide crystallites usually generates heterogeneous composite materials with an uneven

coating. Magnetic nanoparticles formed from the reverse micelle mechanism, where particle size is controlled by the dimension of the micelles, have a more homogeneous morphology but there is an upper limit to the magnetite loading (ca 10% w/w) [6] and the procedure involves the use of large amounts of organic solvents where scale-up is difficult.

A new nanocasting mechanism has been described using ordered mesoporous silica as templates to synthesize iron oxide–silica composites [7]. Many ordered mesoporous silica materials were introduced in the 1990s, notably the MCM (mobile composite materials) [8] and the SBA (Santa Barbara) series [9]. We have reported the preparation of iron(III) oxide–silica (Fe_2O_3–SBA-15) and magnetite–silica (Fe_3O_4–SBA-15 and Fe_3O_4–MCM-48) composite particles using a simple, one-step impregnation with iron(III) nitrate [10] and iron(III) acetylacetonate [11], respectively. Coating this material with short-chain polyethylenimine (PEI) generated particles that delivered higher transfection efficiency than commercial transfection reagents, including Lipofectamine 2000 and Polymag magnetic nanoparticles. However, the iron(III) oxide core of the Fe_2O_3–SBA-15 composite contained a mixture of maghemite and superparamagnetic hematite, while the particle size of the magnetite nanoparticles formed in the case of Fe_3O_4–SBA-15 and Fe_3O_4–MCM-48 exhibited a wide (5–40 nm) size distribution. In order to address these drawbacks, we have developed an enhanced, multi-step synthesis for producing magnetite–silica composites and report herein this new procedure.

2. Experimental methods

2.1. Preparation of SBA-15 mesoporous silica template

SBA-15 mesoporous silica with a long range ordered structure was prepared using the triblock co-polymer Pluronic P123 ($EO_{20}PO_{70}EO_{20}$, BASF) as surfactant template, according to previous literature [12]. A typical gel composition in terms of molar ratio was 1 SiO_2:0.017 P123:2.9 HCl:202.6 H_2O. The surfactant Pluronic P123 was dissolved in an aqueous HCl solution (ca 0.8 M) at 40 °C. Tetraethylorthosilicate (98%, Aldrich) was added to the surfactant solution and the mixture was stirred for 24 h at 30 °C. The mixture was then transferred to a Teflon bottle and heated at 100 °C for 2 days. The resulting white precipitate was filtered and washed with dd H_2O and air dried. The surfactant template was removed by calcining in air at 550 °C for 8 h.

2.2. Impregnation of SBA-15 particles with iron oxide

Iron(III) nitrate ($Fe(NO_3)_3{\cdot}10H_2O$, 99%, Aldrich) was used as the iron precursor. For a 33% w/w iron oxide sample (1 iron(III) oxide: 2 silica by weight), 1.26 g $Fe(NO_3)_3{\cdot}9H_2O$ was dissolved in ethanol (10 cm^3) and 0.5 g of SBA-15 was suspended in the $Fe(NO_3)_3$/ethanol solution. The suspension was left to dry in air at 30 °C overnight with constant stirring. The solid was then subjected to a temperature-programed decomposition (TPD) at a heating rate of 10 °C min^{-1} to 300 °C. This sample is denoted as Fe_2O_3–SBA-15.

2.3. Temperature-programed reduction (TPR) of Fe_2O_3–SBA-15 to form Fe_3O_4–SBA-15, FeO–SBA-15 and Fe–SBA-15

The Fe_2O_3–SBA-15 sample was subjected to TPR using the commercial CHEM-BET 3000 (Quantachrome) unit. The samples were loaded into a U-shaped quartz cell (10 cm × 3.76 mm i.d.) and heated in 20 cm^3 min^{-1} (Brooks mass flow controlled) 5% v/v H_2/N_2 at 10 °C min^{-1} to a final temperature in the range 400–800 °C. The effluent gas passed through a liquid N_2 trap and changes in H_2 consumption were monitored by a thermal conductivity detector (TCD) with data acquisition/manipulation using the TPR WinTM software. The reduced samples were maintained at the final reduction temperature for 90 min in a constant flow of H_2, swept with a 65 cm^3 min^{-1} flow of He for 1 h, cooled to room temperature and passivated in a flow of 1% v/v/O_2 in He.

2.4. Wet reduction of Fe_2O_3–SBA-15 using $NaBH_4$

A solution of 1.5 M $NaBH_4$ was made by dissolving $NaBH_4$ in deoxygenated water. The solution (10 cm^3) was then added to Fe_2O_3–SBA-15 (100 mg) and the particles were suspended for 2 h at room temperature. After reduction, the sample was recovered using an Eppendorf micro centrifuge and washed with deoxygenated water (×3) and air dried at room temperature.

2.5. Characterization techniques

The solid materials were characterized using powder XRD, TEM (JEOL1230 microscope, 100 keV) and magnetometry analysis. The powder XRD patterns (2θ = 10°–80°) were recorded using a Siemens D5000 diffractometer at a scan speed of 0.1° min^{-1}; an alumina sample holder was used. Samples for TEM analysis were suspended in butan-1-ol and deposited on a Formvar/carbon coated copper grid (200 mesh, Agar). Magnetic properties were determined using a commercial Quantum Design MPMS superconducting quantum interference device (SQUID) magnetometer. For a typical measurement, 1 mg of sample was weighed inside a sample capsule. The magnetic moment of the samples was measured between 50 and −50 kOe. There was no correction necessary due to diamagnetic contributions from the sample capsule as they were found to be insignificant.

3. Results and discussion

Our new synthesis approach adopts a temperature-programed reduction (TPR) step, which transforms the iron(III) oxide content into magnetite or metallic iron. This leads to the formation of a homogeneous, superparamagnetic core inside the mesoporous silica template. In our previous work [7], we successfully synthesized Fe_2O_3–SBA-15 nanocomposite particles through a nanocasting preparative route using iron(III) nitrate as an iron precursor. This generated an iron oxide core comprised of superparamagnetic hematite (α-Fe_2O_3) with a lesser superparamagnetic maghemite (γ-Fe_2O_3) content. In order to increase the overall magnetization, the

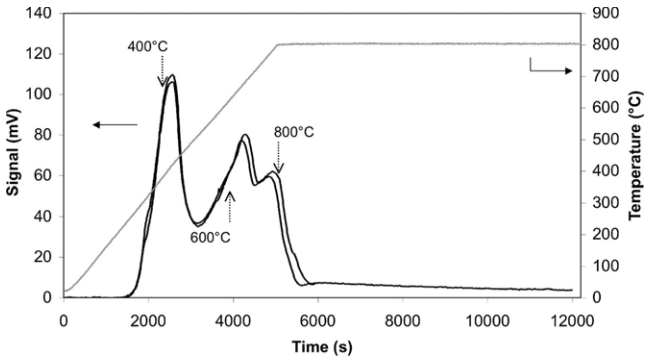

Figure 1. TPR profiles generated for Fe_2O_3–SBA-15. The *y*-axis 'Signal (mV)' label refers to the thermal conductivity response, which is directly related to hydrogen consumption.

particles have been subjected to TPR in flowing H_2 up to three final temperatures, i.e. 400, 600 and 800 °C. The temperature-programed profile taken to the highest temperature is shown in figure 1. Repeated TPR runs are included to illustrate the level of reproducibility. It can be seen that there are three distinct (H_2 consumption) peaks, corresponding to three stages of reduction;

$$Fe_2O_3 \xrightarrow{H_2} Fe_3O_4 \xrightarrow{H_2} FeO \xrightarrow{H_2} Fe. \quad (1)$$

Based on the TPR response, we propose that the sample reduced at 400 °C is predominantly magnetite (Fe_3O_4), iron(II) oxide is obtained after reduction at 600 °C (FeO) and metallic iron is generated after TPR to 800 °C. This sequential reduction has been reported in literature [13]. Measurement of the hydrogen taken up by the composite during TPR has revealed that the amount consumed at 400 °C exceeded that required for the formation of Fe_3O_4 by a factor of 1.3. This result suggests some further reduction of the Fe_3O_4 generated from the starting Fe_2O_3. The hydrogen consumption (2.3 mmol g^{-1}) after TPR to 600 °C is close to that required for the formation of FeO while the value obtained after completion of the TPR (4.0 mmol g^{-1}) closely matches the requirement for complete reduction to metallic Fe. XRD analysis has been used to identify sample composition and the diffraction patterns associated with the samples reduced at 400, 600 and 800 °C are compared (in figure 2) with reference patterns for Fe_3O_4, FeO and Fe. The diffraction pattern for the composite reduced at the lowest reduction temperature (figure 2(a)) shows a strong presence of Fe_3O_4 with some residual Fe formation. The presence of the latter accounts for the 'over consumption' of hydrogen during TPR. The diffractogram (figure 2(b)) for the sample reduced at the intermediate temperature is consistent with a predominant FeO formation and a lesser Fe (and even Fe_3O_4) content. The diffractogram given in figure 2(c) (reduction at 800 °C) is characterized by a strong signal due to the presence of Fe. There is also evidence of iron(II) silicate (Fe_2SiO_4) which can be considered an intermediate in the formation of Fe. Maintaining the reduction temperature at 800 °C for 90 min (figure 2(c)) clearly strengthened the Fe signal, indicating further reduction during this isothermal hold. Based on the

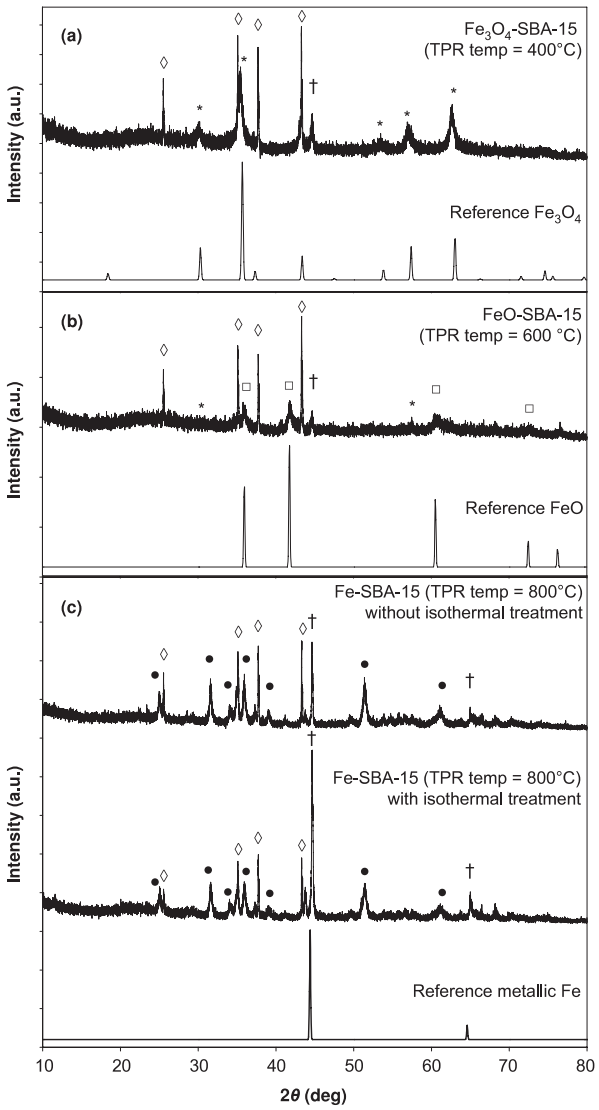

Figure 2. Powder XRD patterns of (a) Fe_3O_4–SBA-15; (b) FeO–SBA-15 and (c) Fe–SBA-15. Reference Fe_3O_4, FeO and Fe patterns are included for comparison. Note: ∗ denotes Fe_3O_4; □ denotes FeO; † denotes metallic Fe; ● denotes Fe_2SiO_4; ◊ denotes peaks due to alumina sample holder.

combined TPR and XRD results, we accordingly label the samples reduced at 400, 600 and 800 °C as Fe_3O_4–SBA-15, FeO–SBA-15 and Fe–SBA-15, respectively.

It should be noted that both Fe_3O_4–SBA-15 (figure 2(a)) and FeO–SBA-15 (figure 2(b)) exhibited weak and wide diffraction peaks, suggesting that the iron oxide particles are at the nanoscale. The stronger signal and sharper peak recorded for the iron metal content in Fe–SBA-15 (figure 2(c)) is diagnostic of metal particle sintering at the higher reduction temperature. The structure and dimensions of the iron oxide/metal–silica composite materials post-TPR were also examined by HRTEM and representative images are shown in figure 3. At all three reduction temperatures, the samples retained the starting 2D hexagonal structure (see figures 3(a.i), (b.i) and (c.i)). In contrast to our earlier work using iron acetylacetonate as the iron precursor [11], the morphology

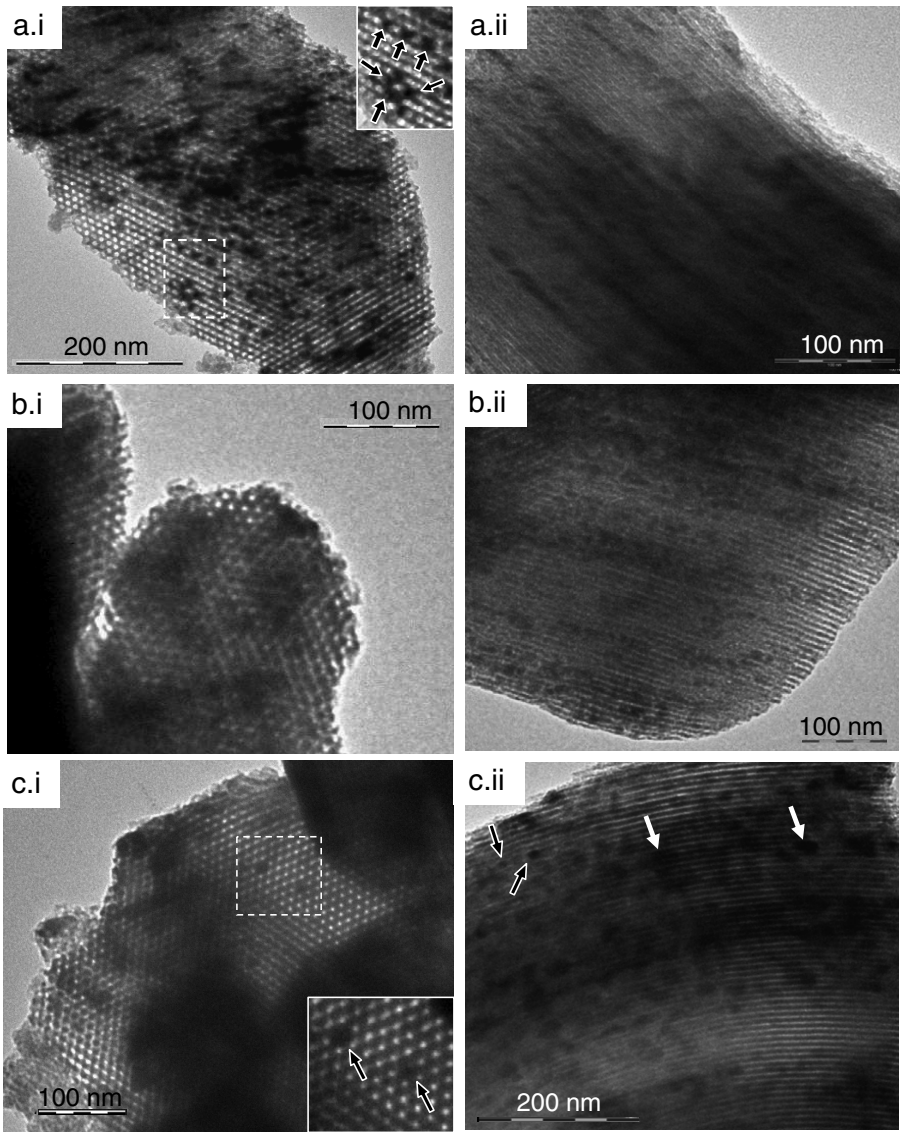

Figure 3. TEM images of Fe_3O_4–SBA-15 ((a.i), (a.ii)), FeO–SBA-15 ((b.i), (b.ii)) and Fe–SBA-15 ((c.i), (c.ii)). The image set (i) demonstrates that the samples retain their 2D hexagonal structure (in cross-section) while set (ii) shows the parallel (lateral) view. The black arrows indicate small magnetite and iron metal particles (about 6 nm) located inside the SBA-15 pore structure while the white arrows indicate larger iron metal particles (about 20 nm) formed in Fe–SBA-15.

of the SBA-15 particles has been preserved. It can be seen in figure 3(a.i) that the magnetite particles are embedded inside the SBA-15 pore network. The inset to this figure provides an enlargement of an area where magnetite particles (indicated by black arrows) are located within the SBA-15 pores. The pore sizes of SBA-15 are in the range 5–8 nm and can accommodate these particles (average diameter = 6.5 nm, based on a measurement of over 50 particles) shown in figure 3(a.i). Once introduced during impregnation, the iron(III) oxide has low mobility and migration to the outer surface during TPR to 400 °C does not occur. From a consideration of the representative TEM images presented in figures 3(b.i) and (b.ii), there was no significant structural disruption after TPR to 600 °C. At a reduction temperature of 800 °C, larger Fe metal particles (up to 20 nm) are formed (see figure 3(c.ii)), a consequence of a temperature induced metal sintering, as suggested by the XRD analysis. In addition to metallic iron particles, iron(II) silicate was also identified from the XRD results. However, as the peaks corresponding to iron(II) silicate are broad and of relatively low intensity, the associated particle size is unlikely to exceed 10 nm. The TEM images reveal the presence of smaller particles inside the pores (indicated by black arrows in figure 3(c.i)) while the sintered particles (indicated by white arrows in figure 3(c.ii)) must result in some local support structural breakdown. Indeed, it is known that the SBA-15 structure can collapse at temperatures greater than 800 °C [14]. The schematic given in figure 4 serves to illustrate the genesis of Fe–SBA-15 from a starting Fe_2O_3–SBA-15 via TPR and provides an idealized rendering of the TEM images from a cross-section and lateral perspective.

The magnetic properties of these nanocomposite particles were studied by SQUID magnetometry and the results are

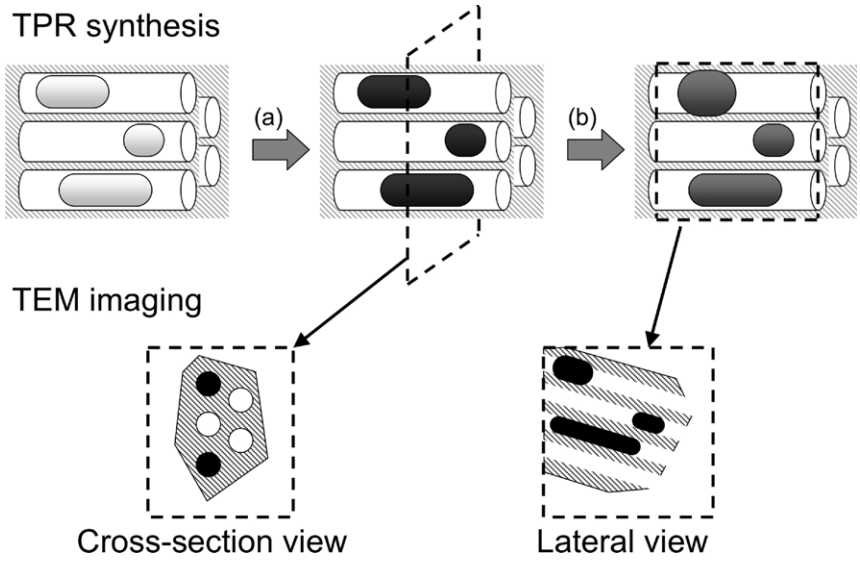

Figure 4. Illustration showing the TPR synthesis of (a) Fe_3O_4–SBA-15 (at 400 °C) and (b) Fe–SBA-15 (at 800 °C) from Fe_2O_3–SBA-15 with associated TEM views.

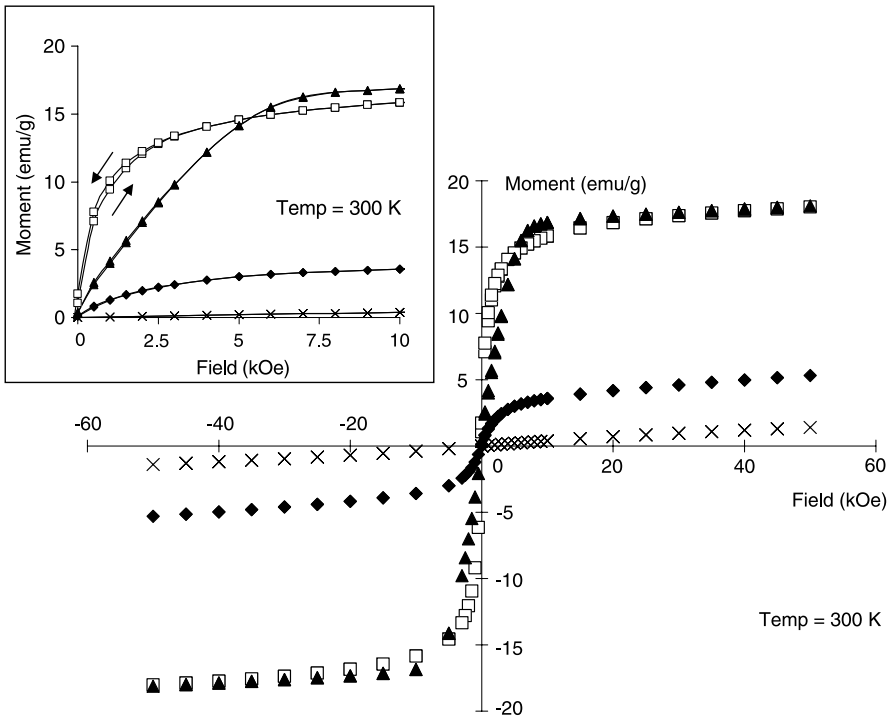

Figure 5. *M* versus *H* plots from SQUID magnetometry measurements at 300 K for samples reduced at (□) 400 °C (Fe_3O_4–SBA-15), (♦) 600 °C (FeO–SBA-15), (▲) 800 °C (Fe–SBA-15) and the unreduced (×) starting Fe_2O_3–SBA-15. The inset shows the magnetization of samples between 0 and 10 kOe and demonstrates the difference in the magnetization curves for Fe_3O_4–SBA-15 and Fe–SBA-15.

presented in figure 5. As we reported previously [10], the starting Fe_2O_3–SBA-15 (prior to reduction) showed typical superparamagnetic properties with 1.5 emu g^{-1} attained at 50 kOe. After TPR to 400 °C, the majority of the iron oxide was reduced to magnetite with a small amount of metallic iron (as confirmed by XRD) and the *M* versus *H* curve shows a sharp increase in magnetization from 0 to 3 kOe with saturation at 4 kOe. This behavior is consistent with that reported in the literature for magnetite [15]. The total magnetization obtained after TPR to 400 °C (17 emu g^{-1}) far exceeded that (5.1 emu g^{-1}) obtained after TPR to 600 °C. The lower value delivered at the higher temperature reduction can be attributed to the formation of FeO from magnetite. Any magnetization in this case must be due to residual magnetite and some metallic iron in the core. When compared with the starting material, the overall magnetization associated with the sample reduced at 400 °C exhibits a

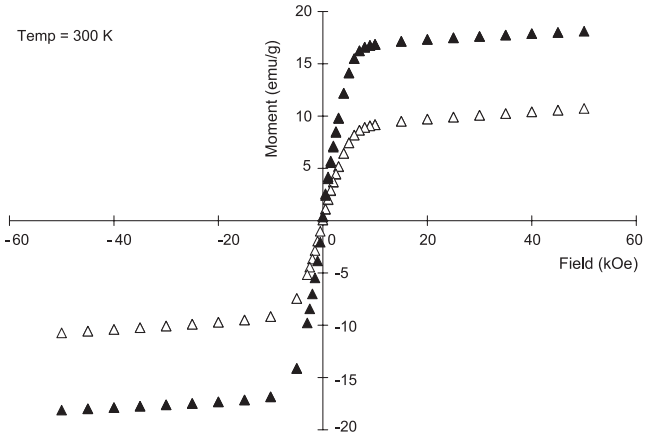

Figure 6. *M* versus *H* plots from SQUID magnetometry measurements of Fe–SBA15 with (▲) and without (△) a 90 min isothermal reduction at 800 °C.

30-fold increase. A magnetization value of ca 45 emu g^{-1} has been reported for magnetite nanoparticles (11 nm), prepared by thermal decomposition of iron pentacarbonyl, which is lower than that (ca 95 emu g^{-1}) for bulk magnetite [16]. The associated specific magnetization value for Fe_3O_4–SBA-15 is ca 52 emu g^{-1} (based on 33% w/w Fe_3O_4 in the composite), which is over 16% higher than the literature value. This is a significant improvement considering the smaller magnetite particle size (6.5 nm) obtained in our sample. On increasing the reduction temperature to 800 °C, iron metal is formed in the core and the overall magnetization was again raised to 17 emu g^{-1}. In contrast to Fe_3O_4–SBA-15, the magnetization associated with Fe–SBA-15 showed a constant increase from 0 to 8 kOe to approach saturation at 8 kOe. This is clearly shown in the inset to figure 5, which expands the magnetization curve from 0 to 10 kOe. The *M* versus *H* plots obtained for Fe–SBA-15 reduced at 800 °C, with and without the 90 min isothermal hold can be compared in figure 6. The additional reduction to Fe achieved during the isothermal treatment, and established by XRD analysis (see figure 2(c)), served to increase the overall magnetization from about 10 to 17 emu g^{-1}. In the literature, α-iron nanoparticles have been reported to exhibit magnetization values of 110 emu g^{-1} (11 nm particles) [17] and 180 emu g^{-1} (35 nm particles) [18]. These values are higher than that achieved in this work, (66 emu g^{-1} Fe (based on a 26% w/w Fe content)) but this may be attributed to the smaller Fe particles formed in Fe–SBA-15 (ca 30% of the Fe particles are in the 5–8 nm range) in tandem with a diamagnetic contribution to the magnetization from the silica matrix. Another source of the lower magnetization value may be the presence of iron(II) silicate, detected by XRD. As an addendum to this work and as an alternative to TPR, 'wet reduction' using strong reducing agents such as $NaBH_4$ or $LiAlH_4$ was also attempted to produce comparable FeO_x-SBA-15 materials. However, we observed an unavoidable rapid oxidation of the magnetic FeO_x-SBA-15 formed post-reduction with a color change from reddish-brown (Fe_2O_3) to blackish-brown (magnetite) and back to reddish-brown within 1 h. It must be stressed that our TPR treatment and subsequent controlled passivation resulted in a stable magnetic product.

Magnetite–silica nanoparticles have been made commercially available in recent years. However, most of these materials only contain about 10% w/w magnetite[6]. As a result, the overall magnetization value is typically 5–7 emu g^{-1}. The Fe_3O_4–SBA-15 prepared via our nanocasting/TPR route delivered an overall magnetization of 17 emu g^{-1}, i.e. up to a three-fold increase relative to commercial products. Given a pore volume of about 1 cm^3 g^{-1} associated with SBA-15 [12], the maximum magnetite loading is estimated to be 83% (based on a density of magnetite = 5 g cm^{-3}). We accordingly predict an upper magnetization of 43 emu g^{-1} for these materials. This level of magnetization is critical in magnetic drug delivery to 'deep organs' as a high magnetization is required to drive magnetic nanoparticles to the target tissues. This is currently a serious obstacle in the development of 'magnetic drug delivery' [2]. In addition to their potential application in the biomedical field [19, 20], these nanocomposites can find possible uses in nanoelectronics and computing, particularly in hard-drive technology and memory storage. We wish to flag one possible extension to this work, adopting thin-film monolith mesoporous silica with pores that are perpendicular to the plane of the film pores [21]. Applying our nanocasting-TPR technology, a 2D hexagonal nanopatterned magnetic-silica 'sheet' or coating may be manufactured. This can then be developed into the next generation of high-density memory system for the computing industry.

4. Conclusions

In summary, this work presents a new strategy, nanocasting/TPR, for the preparation of magnetite–silica and iron–silica nanocomposite materials with high iron contents. The procedure involves limited use of solvent and production scale-up is not difficult. The TPR treatment facilitates control over composite composition in terms of the sequential reduction steps, $Fe_2O_3 \rightarrow Fe_3O_4 \rightarrow FeO \rightarrow Fe$. At a 30% w/w magnetite loading, the Fe_3O_4–SBA-15 composite accommodated oxide particles of mean diameter 6.5 nm within the support pore network to deliver magnetization values that exceeded those reported in the literature and those obtained using commercially available materials. While we have demonstrated applicability in the preparation of magnetite–silica and iron–silica materials, this synthesis strategy can be developed into a generic protocol for preparing other metal–silica nanocomposites including Ag, Cu, and a wide range of alloys.

Acknowledgments

We acknowledge the assistance of Fernando Cardenas-Lizana with the TPR measurements. HHPY thanks BBSRC for his funding. JD acknowledges the support of a Wolfson Foundation—Royal Society Research Merit Award.

[6] Information provided by magnetic nanoparticles suppliers Micromod Germany and Spherotech, USA.

References

[1] Bonnemain B J 1998 *Drug Target.* **6** 167
[2] Berry C C and Curtis A S G 2003 *J. Phys. D: Appl. Phys.* **36** R198
[3] Yoon T J, Yu K N, Kim E, Kim J S, Kim B G, Yun S H, Sohn B H, Cho M H, Lee J K and Park S B 2006 *Small* **2** 209
[4] Pankhurst Q A, Connolly J, Jones S K and Dobson J 2003 *J. Phys. D: Appl. Phys.* **36** R167
[5] McBain S C, Yiu H H P, El Haj A and Dobson J 2007 *J. Mater. Chem.* **17** 2561
[6] Santra S, Tapec R, Theodoropoulou N, Dobson J, Hebard A and Tan W T 2001 *Langmuir* **17** 2900
[7] Delahaye E, Escax V, El Hassan N, Davison A, Aquino R, Dupuis V, Perzynski R and Raikher Y L 2006 *J. Phys. Chem.* B **110** 26001
[8] Kresge C T, Leonowicz M E, Roth W J, Vartuli J C and Beck J S 1992 *Nature* **359** 710
[9] Zhao D Y, Huo Q S, Feng J L, Chmelka B F and Stucky G D 1998 *J. Am. Chem. Soc.* **120** 6024
[10] Yiu H H P, McBain S C, El Haj A J and Dobson J 2007 *Nanotechnology* **18** 435601
[11] Yiu H H P, McBain S C, Lethbridge Z A D, Lees M R and Dobson J 2008 *J. Biomed. Mater. Res.* A submitted
[12] Yiu H H P, Wright P A and Botting N P 2001 *Micropor. Mesopor. Mater.* **44/45** 763
[13] Venugopal A and Scurrell M S 2004 *Appl. Catal.* A **258** 241
[14] Cassiers K, Linssen T, Mathieu M, Benjelloun M, Schrijnematers K, van der Voort P, Cool P and Vansant E F 2002 *Chem. Mater.* **14** 2317
[15] Zaitsev V S, Filimonov D S, Presnyakov I A, Gambino R J and Chu B 1999 *J. Colloid Interface Sci.* **212** 49
[16] Pei W, Kumada H, Natusme T, Saito H and Ishio S 2007 *J. Magn. Magn. Mater.* **310** 2375
[17] Kuroda C S, Shimura T, Maeda M, Tada T, Handa H, Sandhu A and Abe M 2006 *IEEE Trans. Magn.* **42** 3569
[18] Han Y C, Cha H G, Kim C W, Kim Y H and Yang Y S 2007 *J. Phys. Chem.* C **111** 6275
[19] Scherer F, Anton M, Schillinger U, Henkel J, Bergemann C, Kruger A, Gansbacher B and Plank C 2002 *Gene Ther.* **9** 102
[20] Neuberger T, Schopf B, Hofmann H, Hofmann M and von Rechenberg B 2005 *J. Magn. Magn. Mater.* **293** 483
[21] Li F, Wang Z Y, Ergang N S, Fyfe C A and Stein A 2007 *Langmuir* **23** 3996